Planetary climate systems II

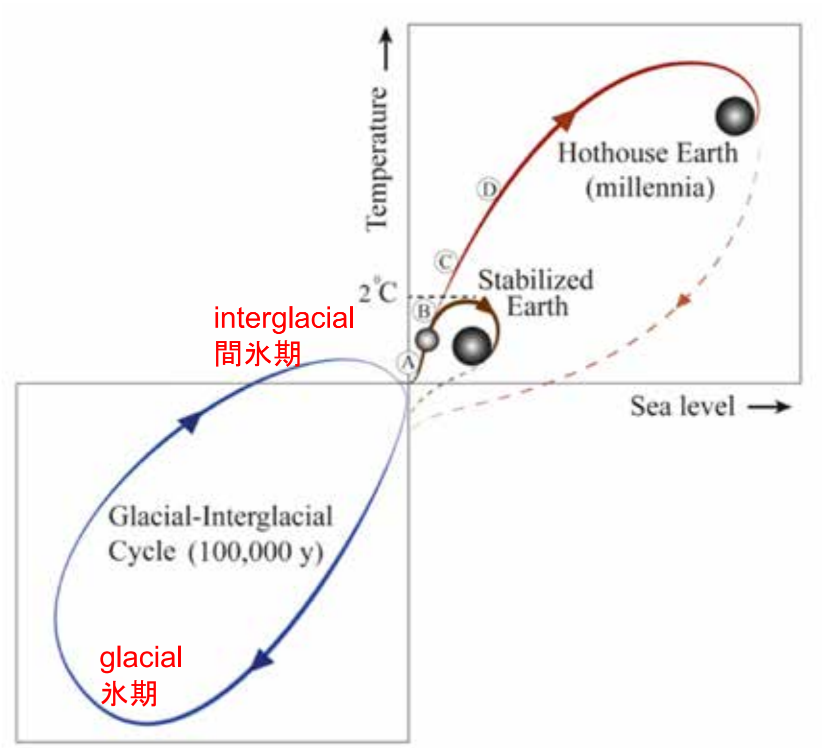

Steffen et al. (PNAS, 2018)

Milankovitch cycles on Mars and Earth

Table 12.10 The orbital elements of Mars and the Earth and their variability.

Parameter	Present Mars	Martian variability		Present Earth	Terrestrial variability	
		Range	Cycle (years)		Range	Cycle (years)
Obliquity (°)	25.19	0–85*	120 000**	23.45	22–24	41 000
Eccentricity	0.093	0–0.12	120 000***	0.017	0.01–0.04	100 000
Longitude of perihelion (°)	250	0–360	51 000	285	0–360	21 000

* Before ~10 Ma, obliquity variations are chaotic. While unpredictable at an exact time, statistically they would have varied between 0 and 85° (Laskar *et al.*, 2004; Touma and Wisdom, 1993).
** The amplitude of obliquity oscillation is modulated with a ~1.2 Myr period envelope.
*** The amplitude of eccentricity oscillation is modulated with a ~2.4 Myr period envelope.

Catling & Kasting 2017

Milankovitch cycle

from Wikipedia

low summer insolation in the northern high latitude
→ growth of ice sheets → **glacial inception (ice age)**

Precession 歳差

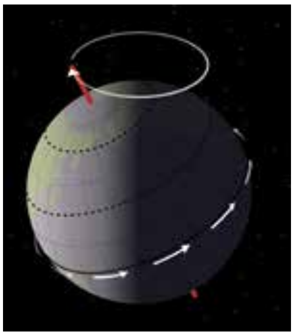

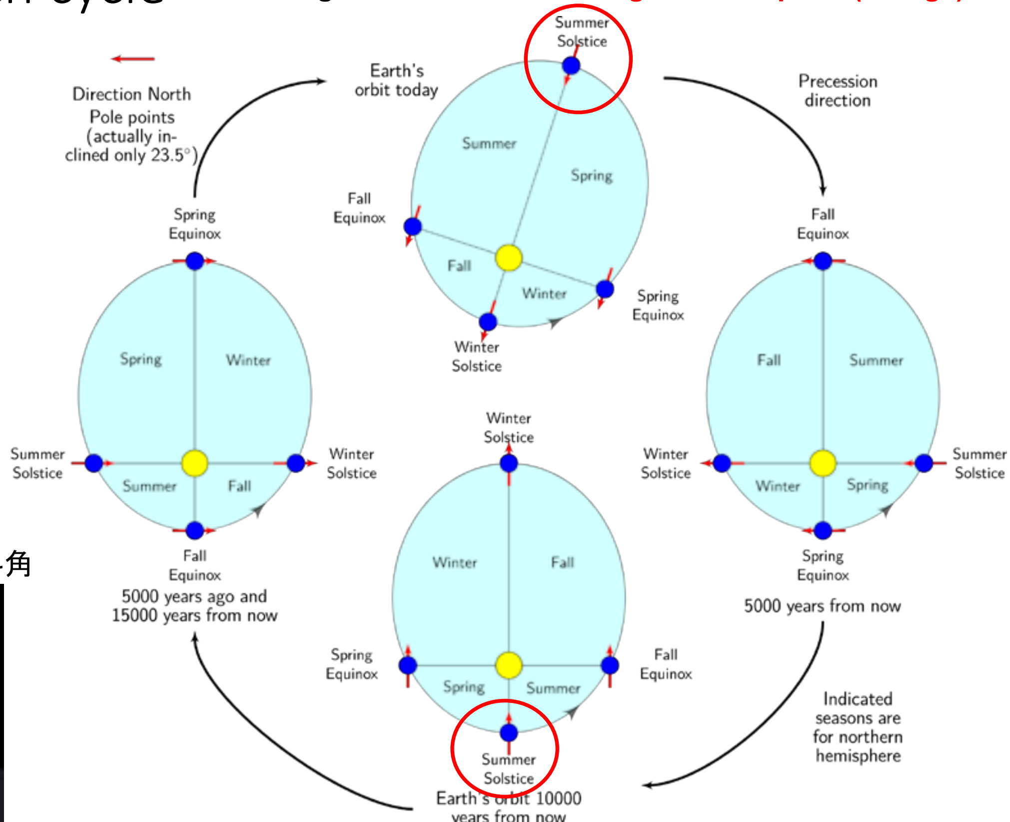

Obliquity 自転軸傾斜角

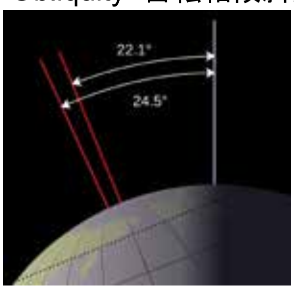

high summer insolation in the northern high latitude
→ decay of ice sheets → **Interglacial (warm interval)**

Glacial inception by CO_2 emission

Ganopolski et al. 2016, Nature

- Interglacials occur during periods of high summer insolation in the high latitudes of the Northern Hemisphere. (Milankovitch theory)
- In the past, a decrease in Northern Hemisphere insolation to below its present-day level always led to the end of interglacials and rapid growth of continental ice sheets.
- However, at present, although summer insolation at 65°N is close to its minimum, there is no evidence for the beginning of a new ice age.
- Glacial inceptions have occurred in the past under similar orbital configurations.

- The current interglacial would have ended if the CO_2 concentration had stayed at a level of about 240 parts per million (ppm), as was the case at the end of MIS19 (800 kyr BP). However, during the late Holocene (完新世：現代含む) before the beginning of the industrial era, the CO_2 concentration was about 280 ppm, leading to escape from glacial inception.
- It has been proposed that pre-industrial land-use at least partly contributed to the high Holocene CO_2 level.
- If carbon emission continues, glacial inception is very unlikely within the next 100,000 years. Anthropogenic interference will make the initiation of the next ice age impossible.

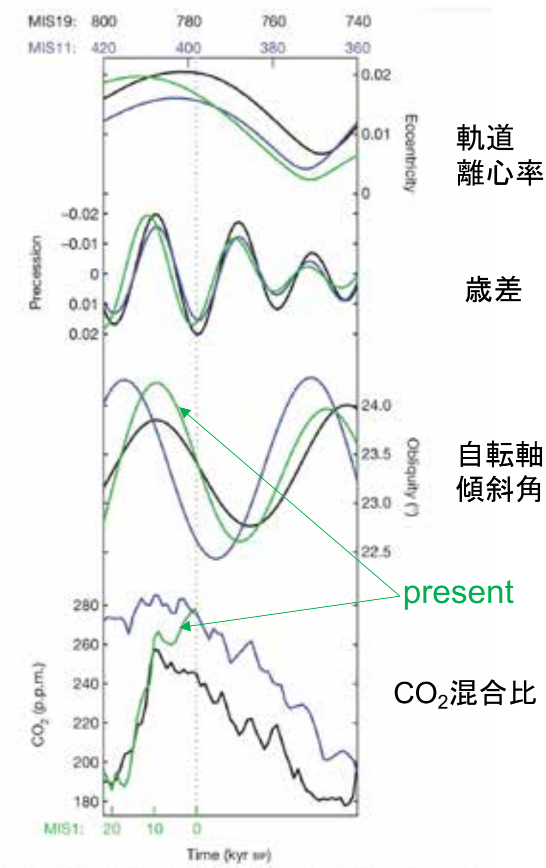

Figure 1 | Orbital parameters. Comparison of Earth's orbital parameters and CO_2 concentrations for MIS1 (green), MIS11 (blue) and MIS19 (black). The vertical dashed line corresponds to the present day for MIS1 and the minima of the precessional component of insolation for MIS11 and MIS19.

Mars

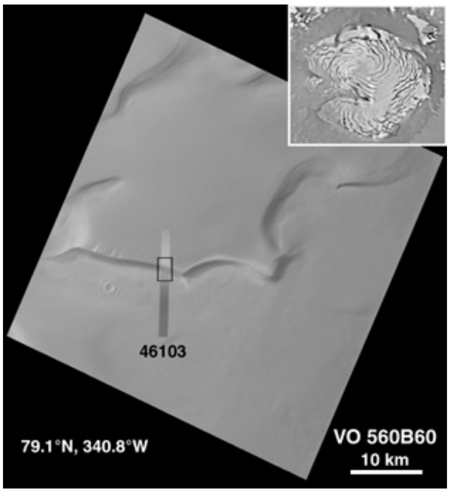

Polar cap deposits

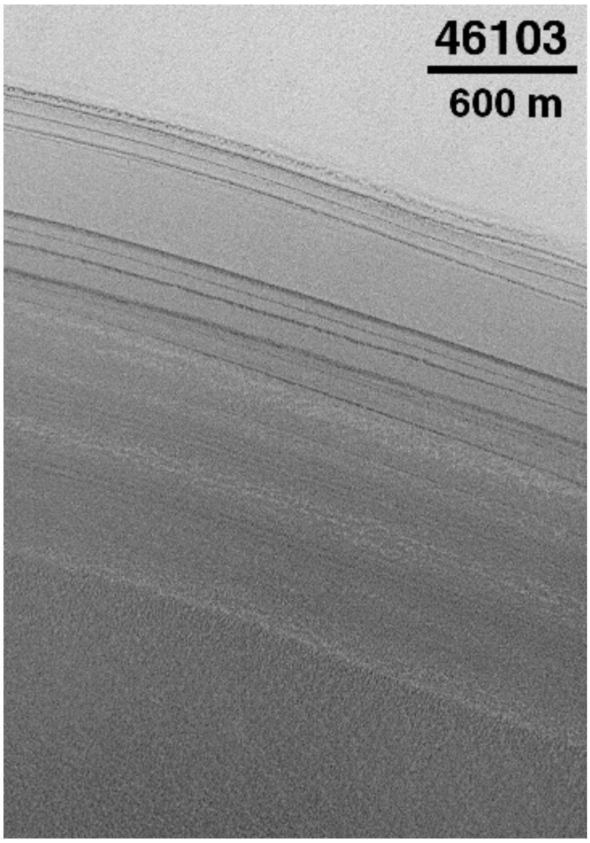

recurrent slope lineae

- transition between different climate regimes ?

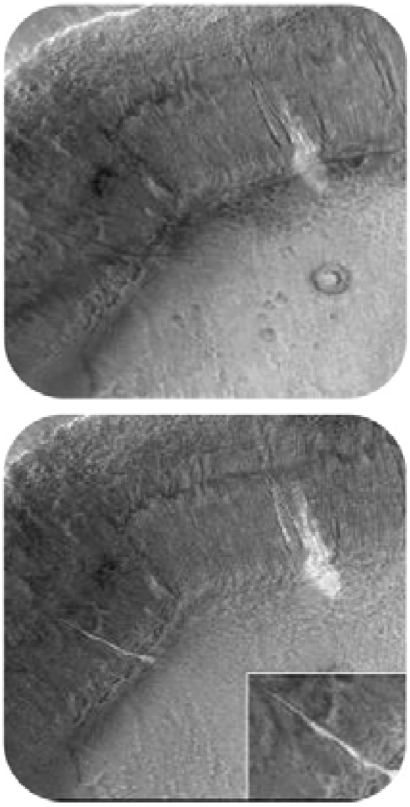

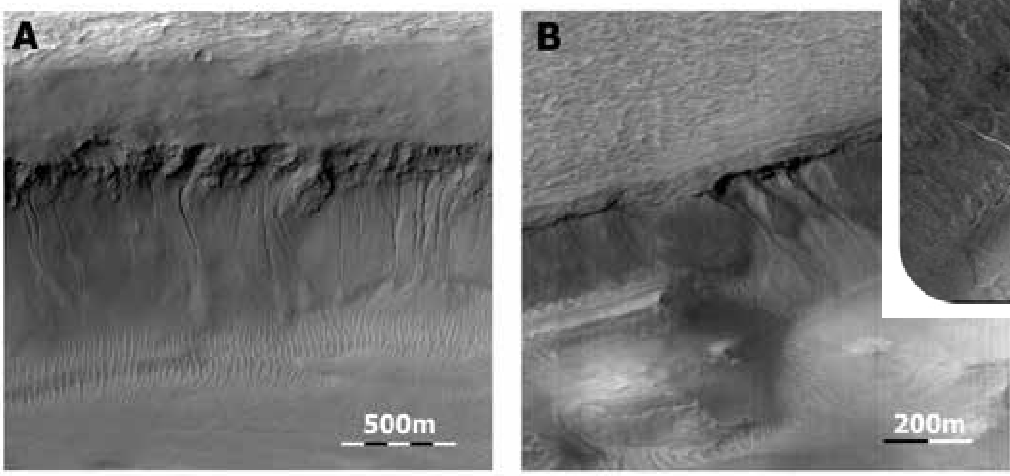

Subsurface ice

Mars Odyssey
Neutron Spectrometer (NS) and High-Energy Neutron Detector (HEND)

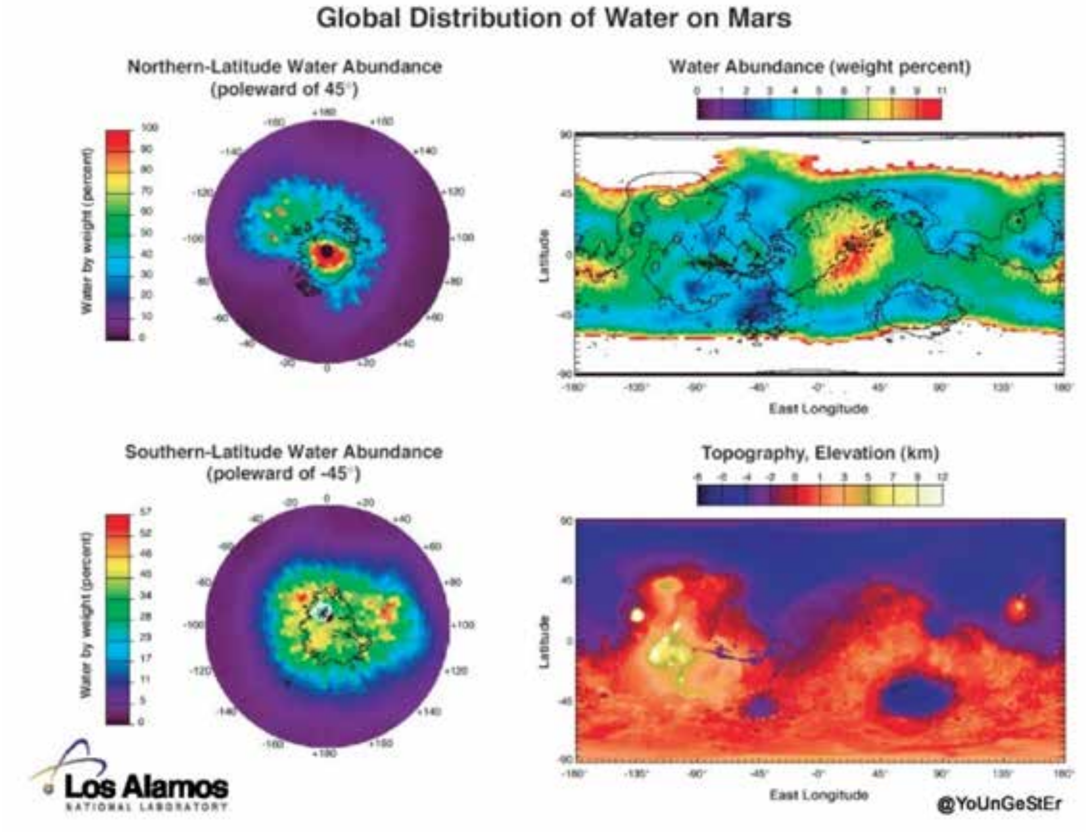

Schorghofer and Aharonson (2005)

Comparison with models

Near equilibrium at high latitudes ?

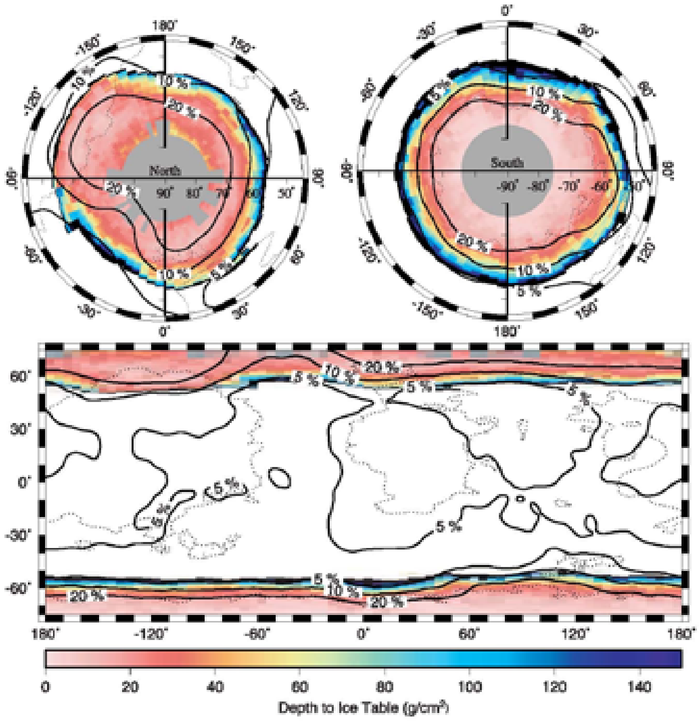

Figure 8. Color indicates depth to the ice table in g cm^{-2} when ice is in equilibrium with the atmospheric water vapor. Ground ice is unstable in the white area. Black segments indicate finite burial depths larger than 150 g cm^{-2}. Missing data points are shown in gray. Assumed volume fraction of ice is 40%, but the geographic boundary between icy and ice-free soil is independent of the ice fraction. Solid contours indicate water-equivalent hydrogen content in percent determined from neutron spectroscopy [*Feldman et al.*, 2004]. The dotted lines are 200 J $m^{-2}K^{-1}s^{-1/2}$ contours of thermal inertia.

色：　大気中の水蒸気との平衡状態を仮定して計算される氷床までの深さ

実線：　中性子分光観測から見積もられた水含有量

Milankovitch cycles on Mars and Earth

Table 12.10 The orbital elements of Mars and the Earth and their variability.

Parameter	Present Mars	Martian variability		Present Earth	Terrestrial variability	
		Range	Cycle (years)		Range	Cycle (years)
Obliquity (°)	25.19	0–85*	120 000**	23.45	22–24	41 000
Eccentricity	0.093	0–0.12	120 000***	0.017	0.01–0.04	100 000
Longitude of perihelion (°)	250	0–360	51 000	285	0–360	21 000

* Before ~10 Ma, obliquity variations are chaotic. While unpredictable at an exact time, statistically they would have varied between 0 and 85° (Laskar *et al.*, 2004; Touma and Wisdom, 1993).
** The amplitude of obliquity oscillation is modulated with a ~1.2 Myr period envelope.
*** The amplitude of eccentricity oscillation is modulated with a ~2.4 Myr period envelope.

Catling & Kasting 2017

Milankovitch cycles on Mars

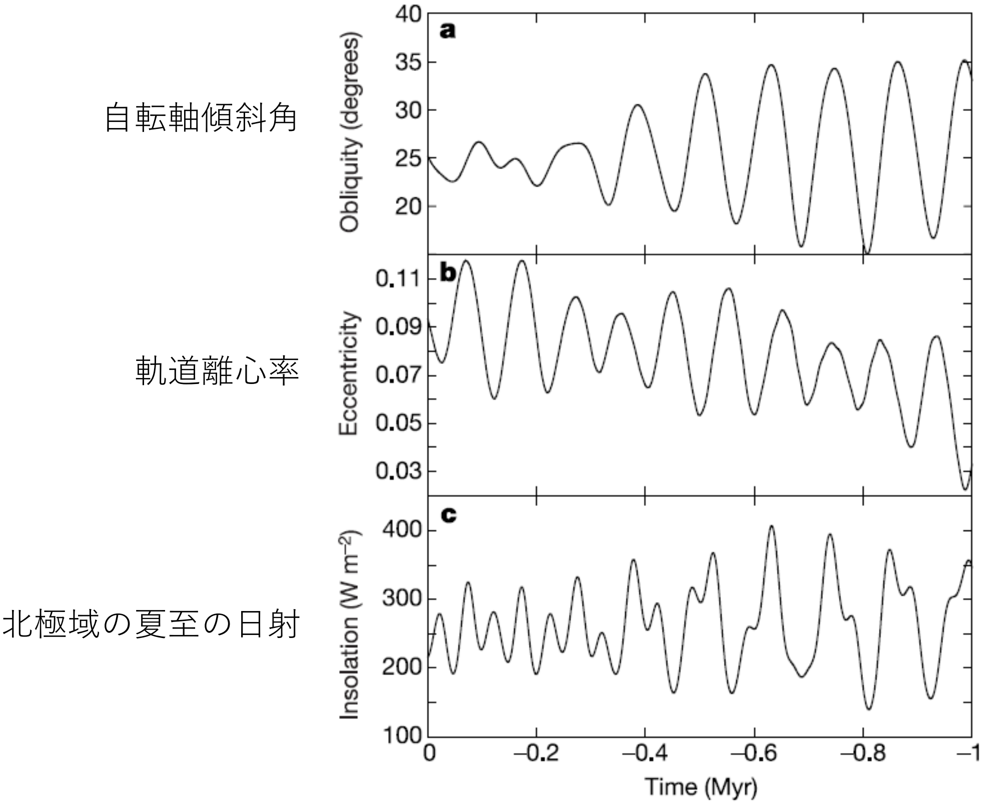

Laskar et al. (2002)

Seasons of Mars

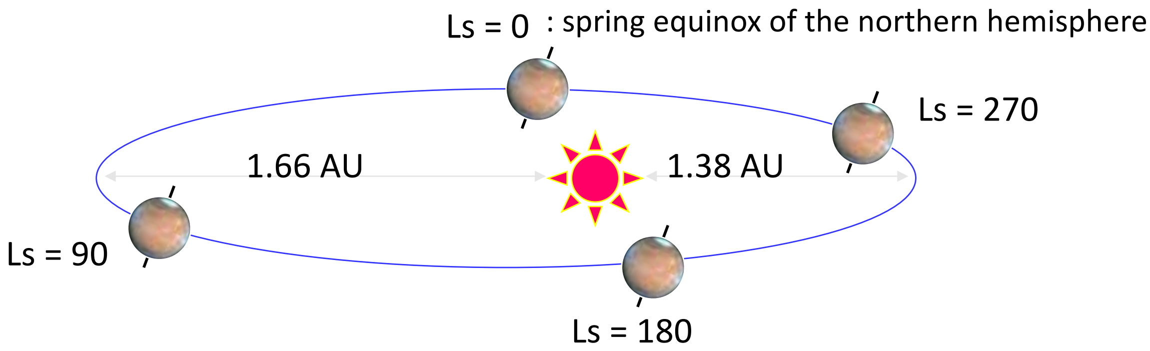

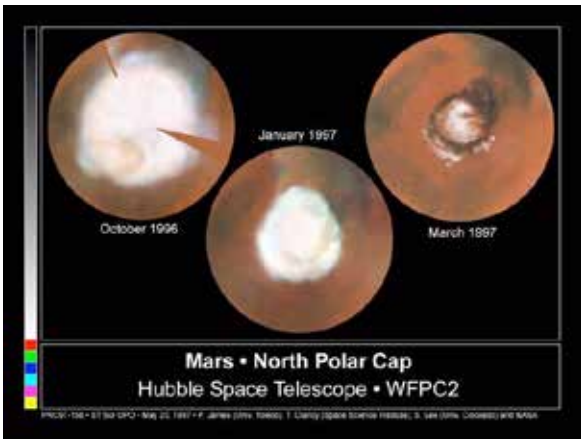

- 火星は公転軌道の離心率が大きいため季節変化が著しく南北非対称
- 南半球の夏に太陽までの距離が近くなる

Kieffer and Zent (Kieffer et al. eds, Univ. Arizona Press, 1992)

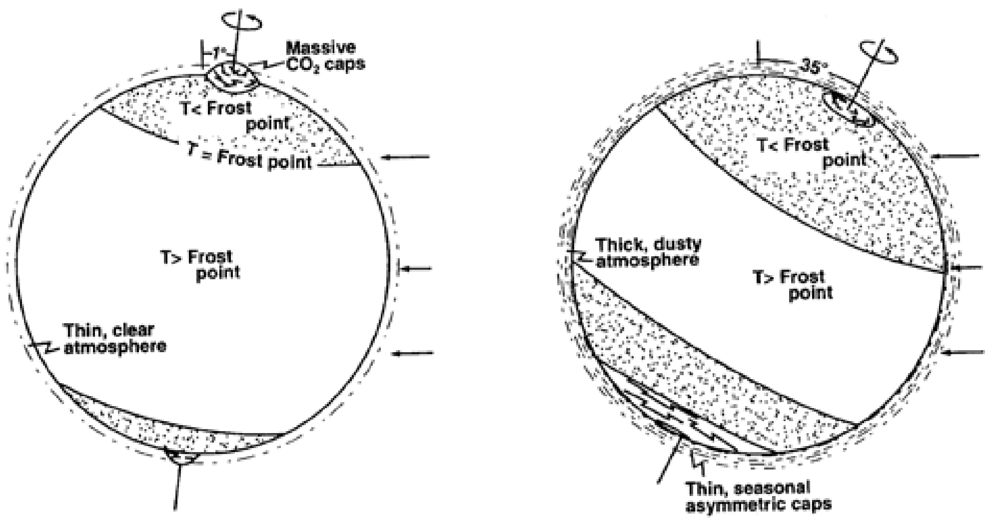

- low obliquity → cold pole → massive polar cap → dry atmosphere → retreat of ice sheet
- high obliquity → warm pole → thin polar cap → moist atmosphere → growth of ice sheet, ice accumulation in the tropics

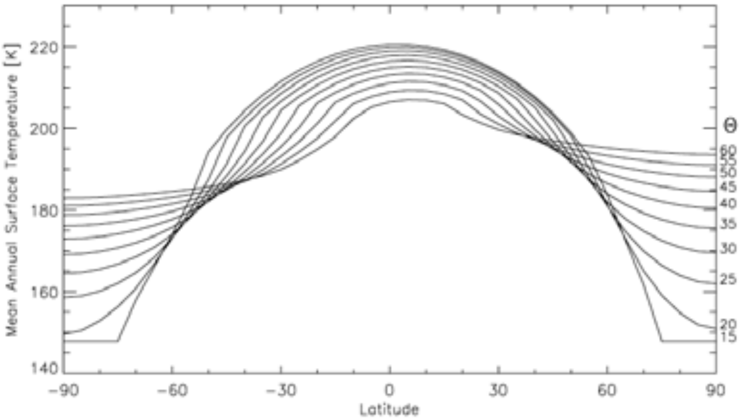

Figure 3. Mean annual surface temperature for a range of obliquities. The eccentricity is 0.12, and the L_S at which perihelion occurs is 270, corresponding to southern summer. A thermal inertia of 250 J m^{-2} $s^{-1/2}$ K^{-1}, an albedo of 0.25, a surface pressure of 600 Pa, and an infrared dust opacity of 0.1 are assumed. Discontinuities in the slope of each curve are due to the effects of seasonal CO_2 frost.

Mellon & Phillips (2001)

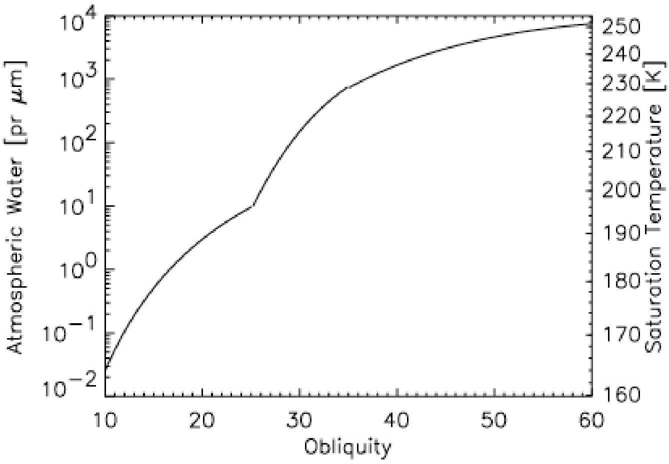

Formation of glaciers on Mars by atmospheric precipitation at high obliquity   Forget et al. (2006)

- The model predicts ice accumulation in regions where glacier landforms are observed, on the western flanks of the great volcanoes and in the eastern Hellas region

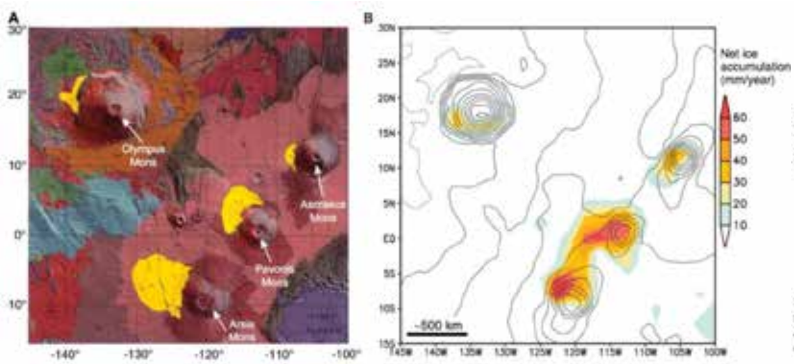

Fig. 1. (**A**) Geologic map modified from (30) of the Tharsis region showing the location of fan-shaped deposits of Amazonian age (yellow) located on the northwest slopes of the Tharsis Montes and Olympus Mons. (**B**) Net surface water ice accumulation in the Tharsis region simulated with 45° obliquity and assuming that surface water ice is present on the northern polar cap. Superimposed Mars Orbiter Laser Altimeter (MOLA) topography contours are at 2000-m intervals. (**C**) Same as (**B**) but for the Elysium Mons region. Outside the Tharsis and Elysium areas, no net ice accumulation is predicted.

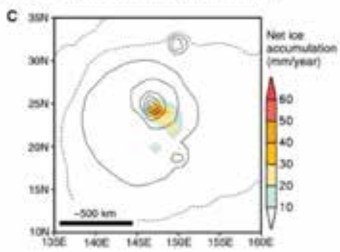

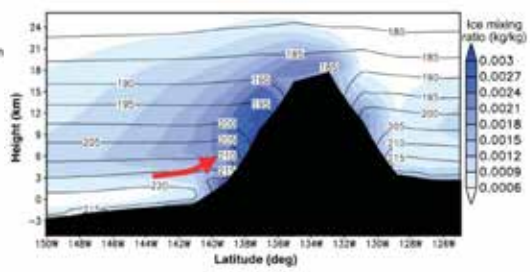

Fig. 3. Cross section of Olympus Mons along the 16°N latitude showing the mean atmospheric ice mass mixing ratio (shaded blue) and the atmospheric temperature (contour, K) averaged over the period of ice accumulation Ls = 125° to 155° (northern summer). The strong northwesterly winds induce adiabatic cooling on the flank of the volcanoes and atmospheric condensation and precipitation.

Buried glaciers

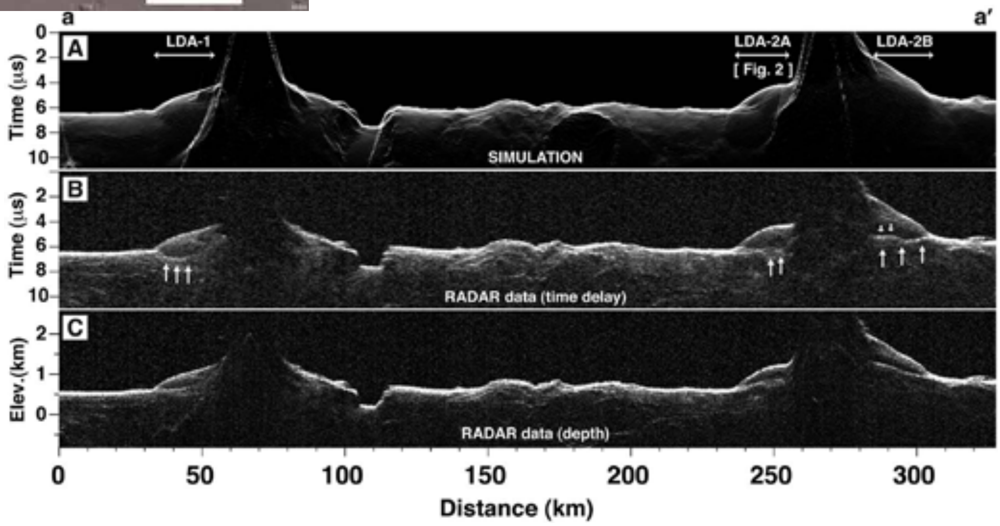

Water transport by Hadley circulation

- Warmer southern summer than northern favors net northward transport of water.

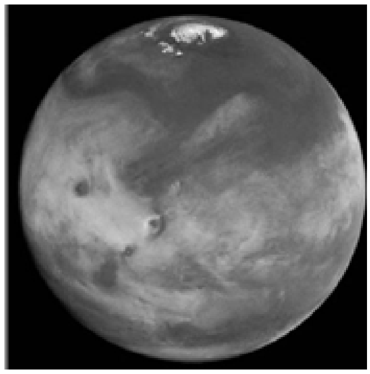

Distribution of H_2O in a Mars GCM

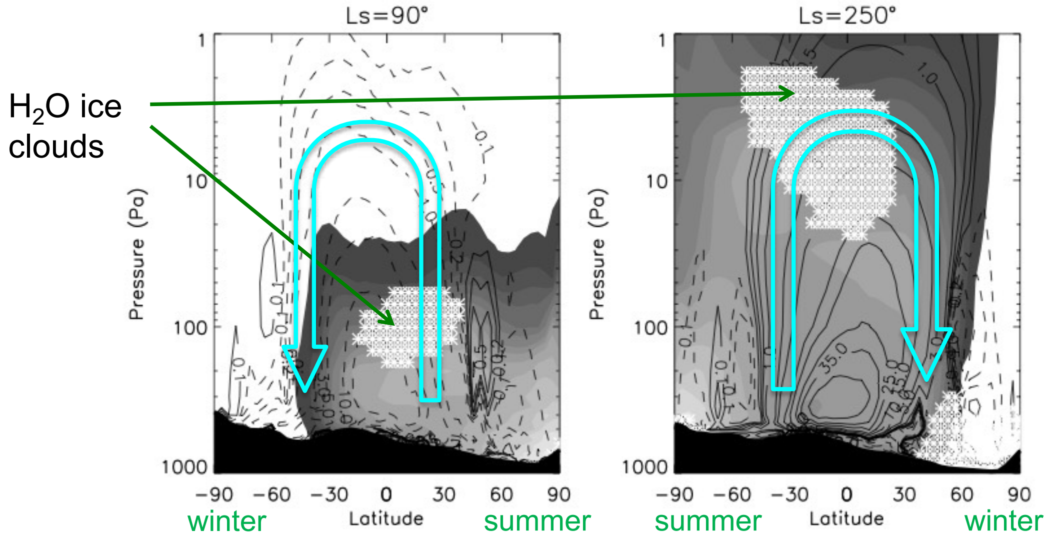

Montmessin et al. (2004)

Seasonal variation of dust, clouds, and H_2O vapor observed by an infrared spectrometer (TES) on Mars Global Surveyor

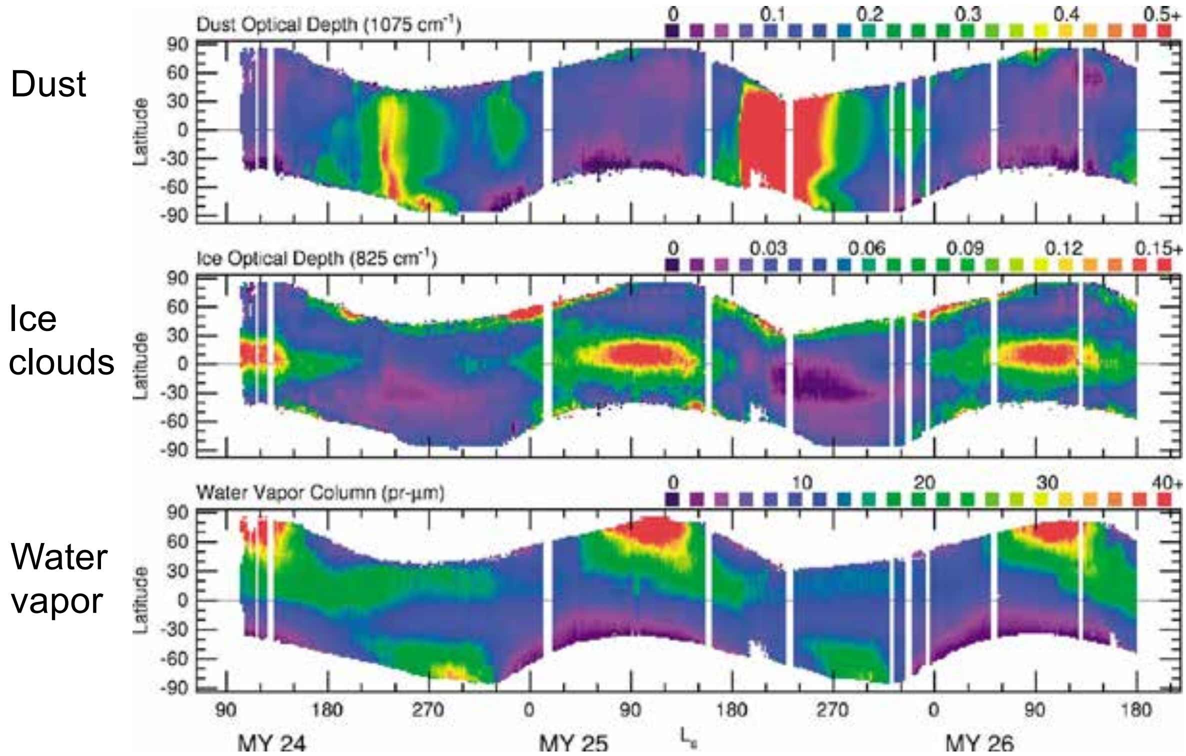

Smith, Icarus 167 (2004) 148–165

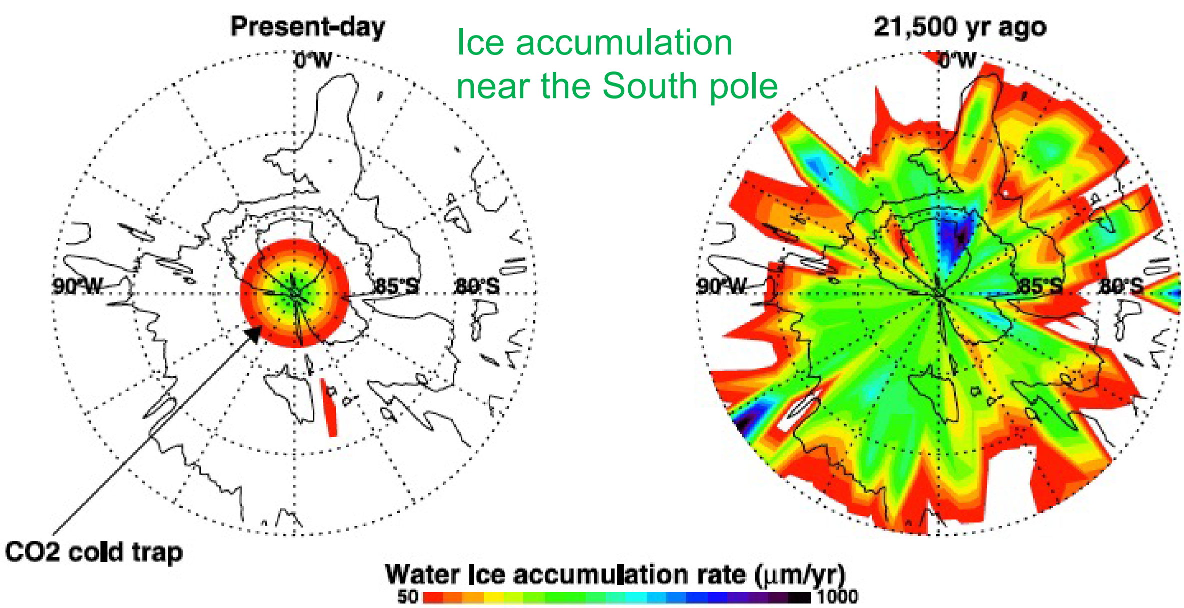

Figure 5. A comparison of water ice accumulation rates predicted by the model in the south polar region for the two perihelion configurations. Present-day map shows net accumulation only at the south pole itself (equivalent to 1 grid point in the model) where the prescription of a CO_2 cold trap forces a local and permanent deposition of water ice. In the reversed perihelion simulation (Figure 5, right), the CO_2 cold trap has been removed and the pattern of accumulation is only controlled by a precipitation versus sublimation positive balance on an annual average.

Supersaturation of water vapor on Mars

SPICAM on Mars Express (Maltagliati et al. 2011)

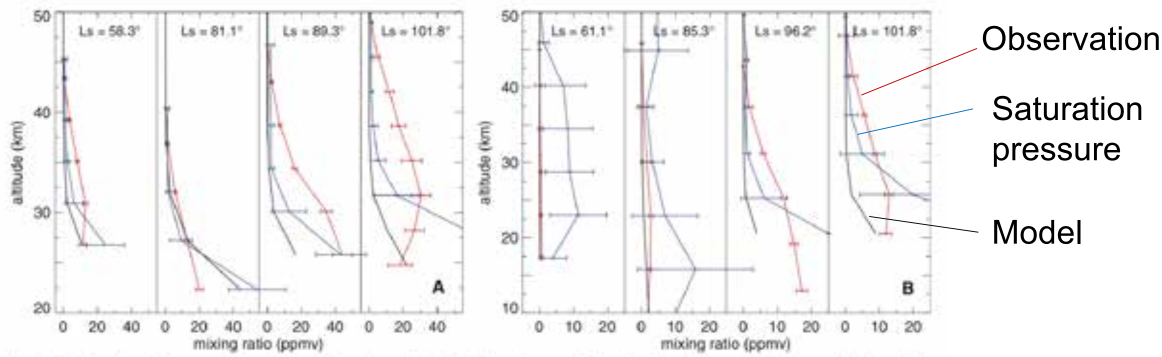

Fig. 2. Selection of typical water vapor volume–mixing ratio profiles in the (**A**) northern and (**B**) southern hemisphere. Black curve, modeled profile by the LMD-GCM; red curve, the retrieved SPICAM results; blue curve, saturation water vapor–mixing ratio. Supersaturation exists where the red values are greater than the blue ones.

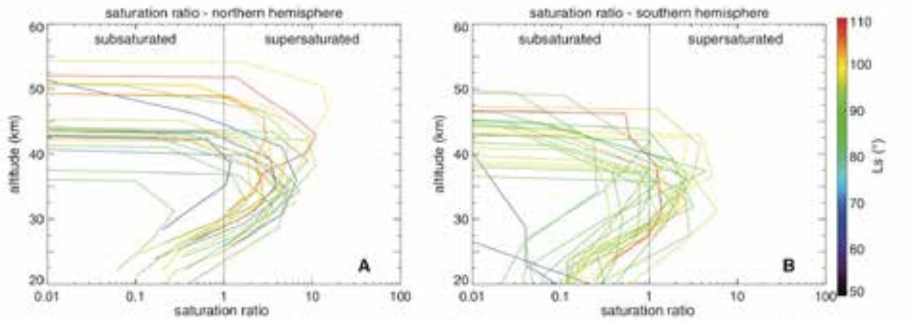

Fig. 3. Saturation ratio for all orbits of the campaign. (**A**) Northern hemisphere. (**B**) Southern hemisphere. The vertical line marks the value of 1, which corresponds to the saturated state.

Global dust storm

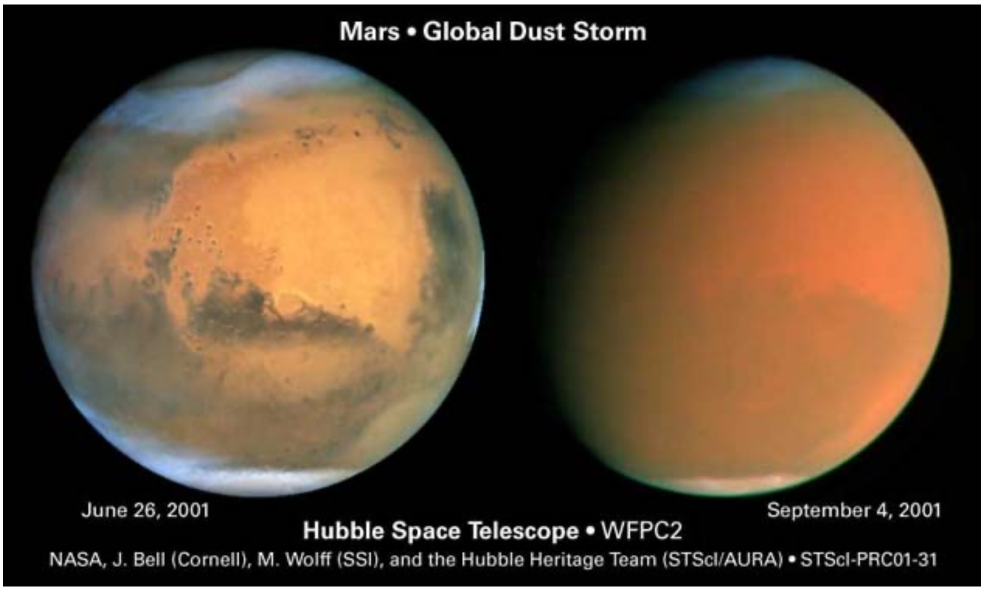

- Global dust storms tend to occur in southern spring-summer
- Positive feedback between dust heating and the intensification of winds is expected in the development of global dust storms.

Episodic occurrence of major dust storms
→ irregular nature of Martian meteorology

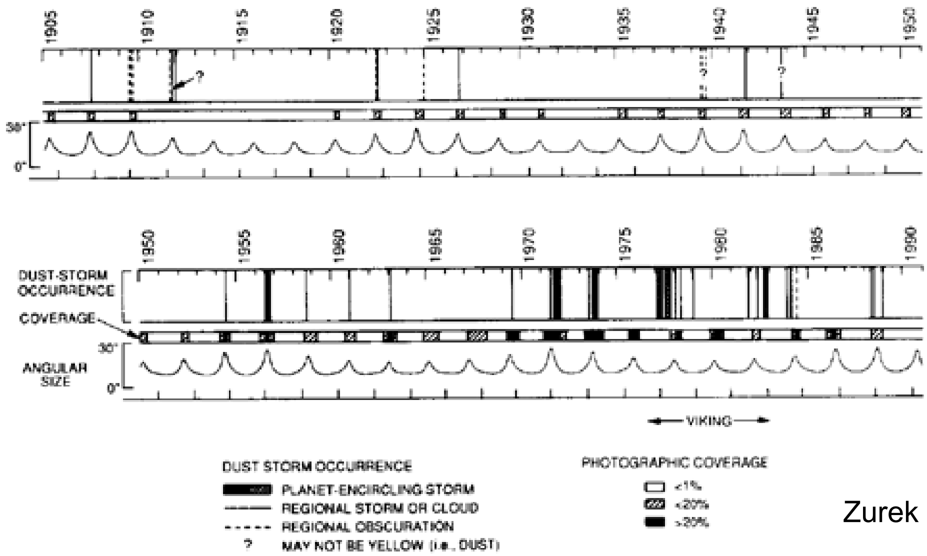

Zurek and Martin, 1993

Fig. 7. Timeline of the detection of regional and planet-encircling obscurations, clouds and storms. These events are listed in Table III. Earth dates are indicated at the top, and perihelion (and thus Mars years) at the bottom of the dust-storm timeline. The second timeline indicates periods of photographic coverage of Mars, defined in terms of the percentage of L_s degrees that photographs were taken. Coverages of <1%, of 1 to 20% and >20% are indicated. The third timeline indicates the apparent size of Mars, as seen from Earth, on a scale of 0 to 30 seconds of arc (figure from Zurek and L. Martin 1992).

H_2SO_4 clouds of Venus

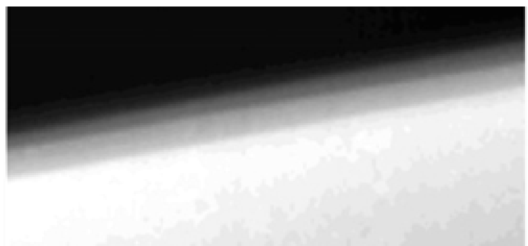

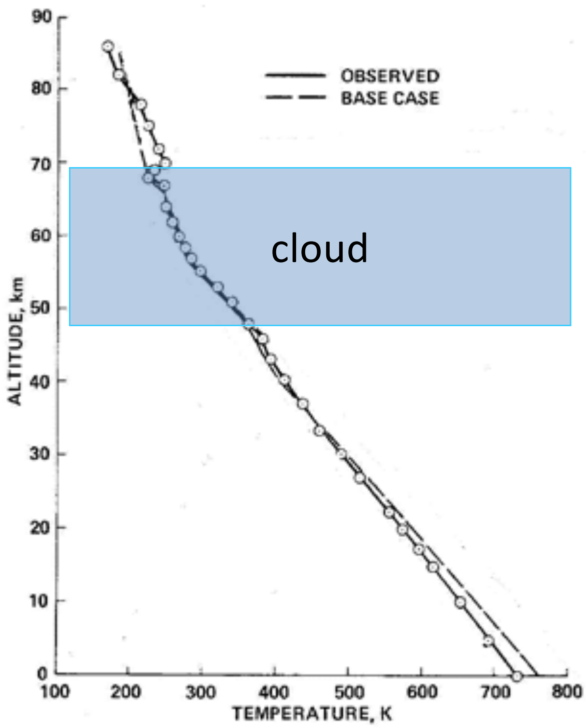

Fig. 2. Comparison between the observed temperature structure of Venus' lower atmosphere and that of several models, which are described in the main text.

- Solar energy flux reaching the Venus surface ($17 W/m^2$) is much less than that of the Earth ($168 W/m^2$).
- Greenhouse effect of massive CO_2 and small amount of H_2O explains the high temperature.

Pollack et al. (1980)

Origin of clouds

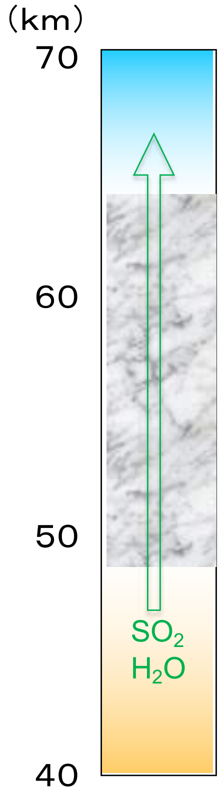

Photochemistry above clouds

Scenario #1 (Net reaction driven by catalytic cycles including ClOx, HOx, NOx)

$$2CO_2 + h\nu \rightarrow 2CO + O_2$$
$$CO + SO_2 + O_2 + h\nu \rightarrow CO_2 + SO_3$$
$$\overline{CO_2 + SO_2 + h\nu \rightarrow CO + SO_3}$$

Scenario #2

$$SO_2 + h\nu \rightarrow SO + O$$
$$SO + h\nu \rightarrow S + O$$
$$SO_2 + O \rightarrow SO_3 \quad (\times 2)$$
$$\overline{3\,SO_2 + h\nu \rightarrow S + 2SO_3}$$

- SO_3 rapidly reacts with H_2O: $\boxed{SO_3 + H_2O \rightarrow H_2SO_4}$
- Elemental sulfur (S) can serve as condensation nuclei.

Variability of SO_2 above clouds

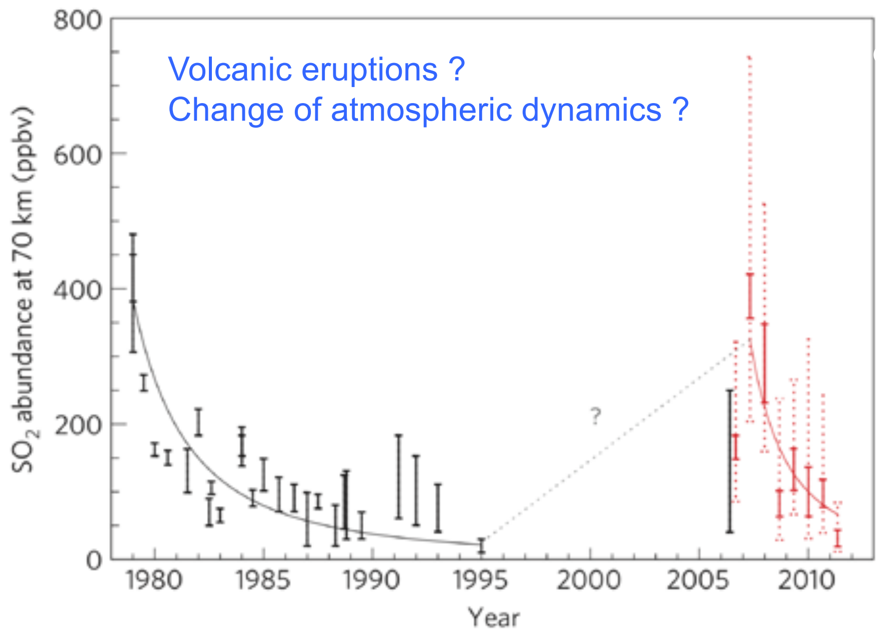

Marcq et al. (2013)

Figure 3 | More than thirty years of SO_2 measurements at Venus's cloud top. Black stands for previously published measurements[26]. Red stands for the 8-month moving average of the retrievals also shown in Fig. 1. Solid red error bars represent 1σ random uncertainty, and dotted red error bars represent measurement dispersion in each temporal bin.

Correlation between UV contrast and SO_2 density ? (Lee et al. 2015)

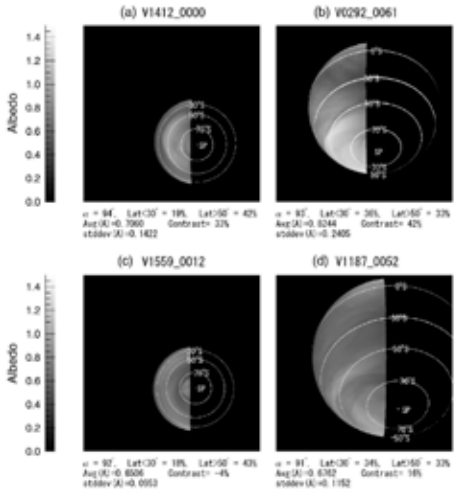

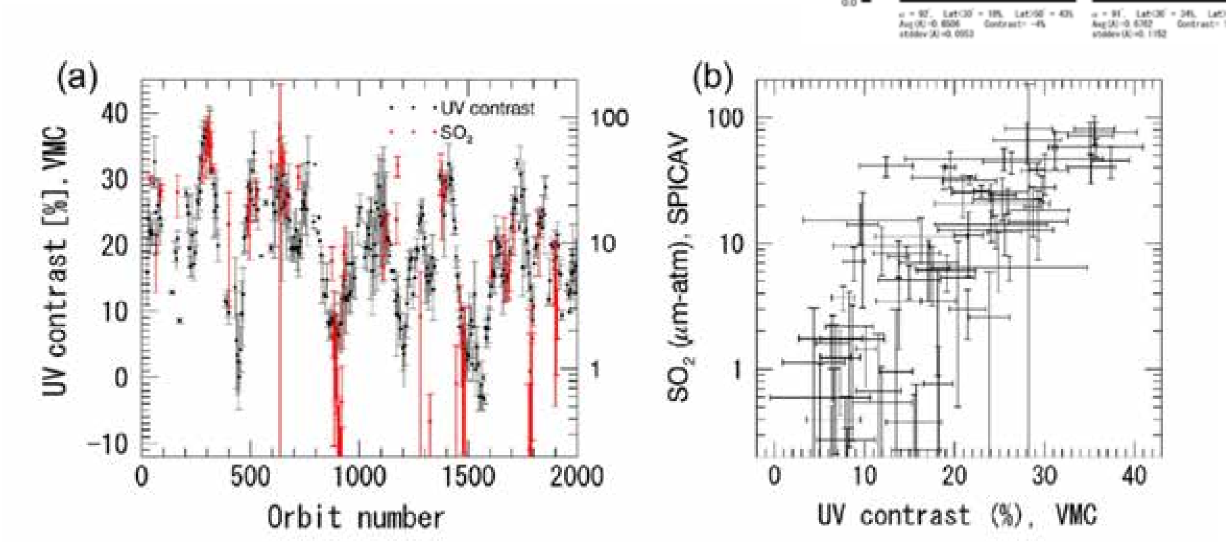

Long-term variations of the UV albedo of Venus (Lee et al. 2019)

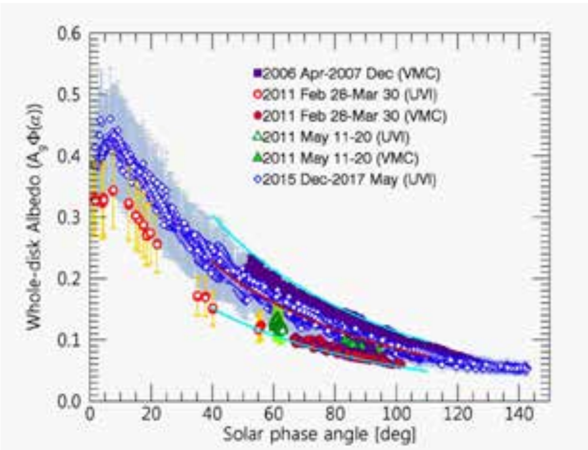

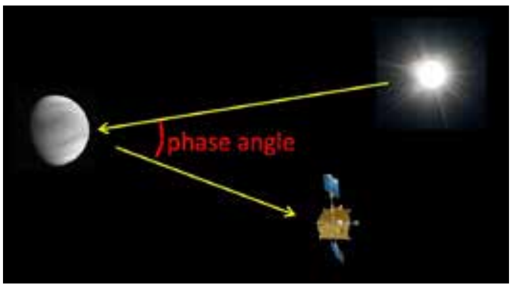

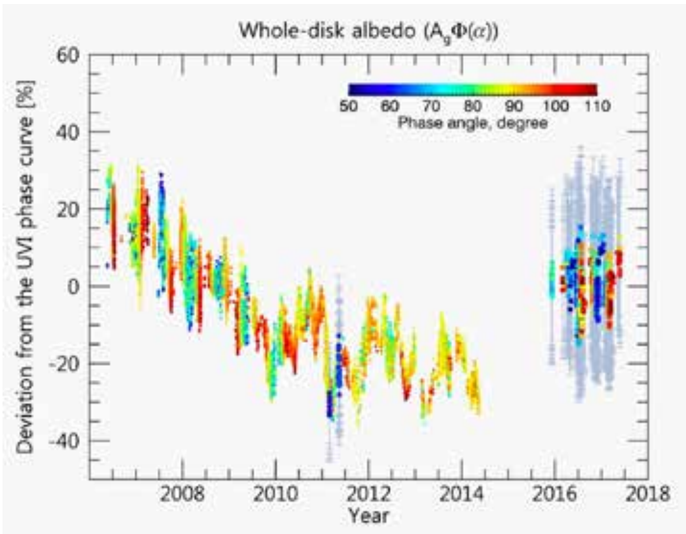

long-term variation of zonal wind in deep clouds

(Peralta et al. 2018)

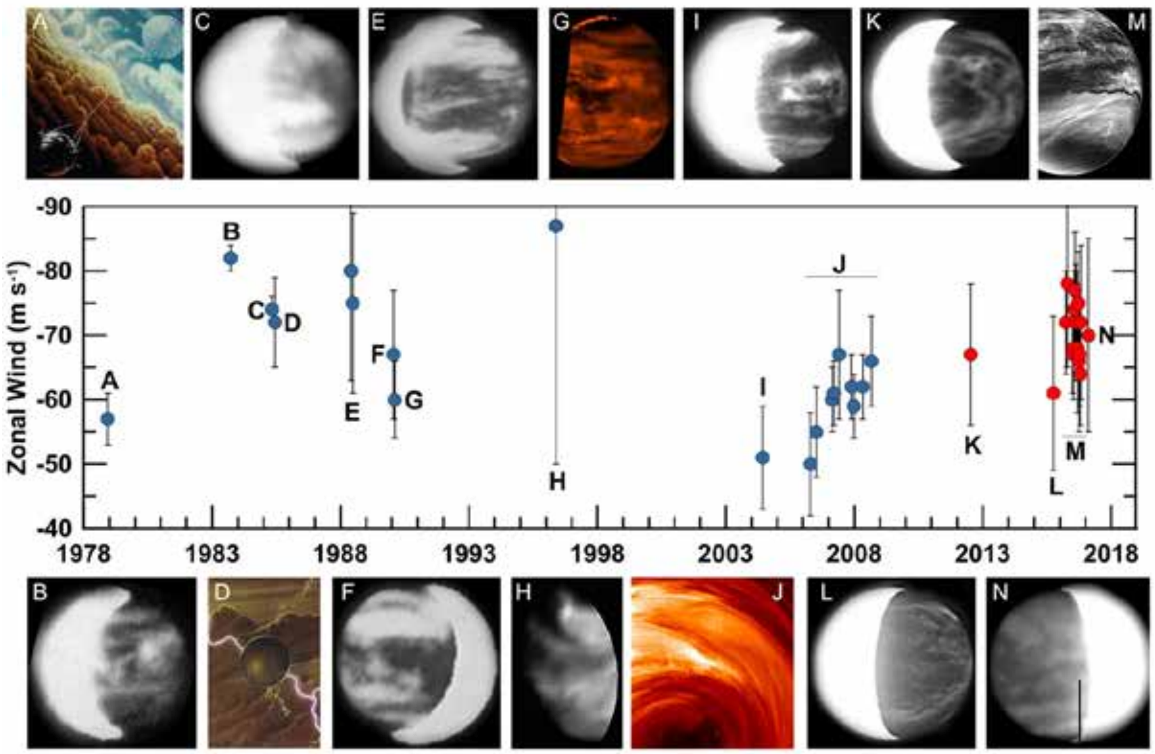

Radiative relaxation time

- Times cale of infrared cooling/solar heating
- The meridional overturning time is usually considered to be similar to the radiative relaxation time.

- Radiative relaxation time is longer for larger atmospheric heat capacities.
  - Mars : 3 Earth days
  - Earth : 100 Earth days
  - Venus : 50 Earth years

* The dynamical time scale of Venus's atmosphere can also be very long → Internal oscillation ?

Spontaneous oscillation of the atmosphere

- Earth : Quasi-biennial oscillation（QBO）

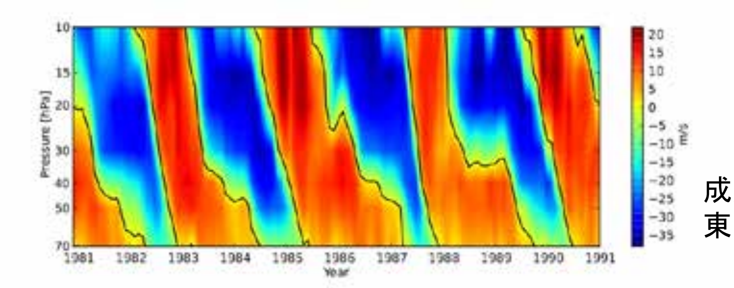

成層圏中下部(高度31～17km付近)の東西風速分布の断面図 (Wikipedia)

- システム内部の素過程の相互作用の手がかり

- 惑星では、木星の準4年振動（QQO）、火星のglobal dust stormの不定期発生、金星のスーパーローテーションの年々変動　など